

Microwave Observations of Edge-on Protoplanetary Disks: Program Overview and First Results

Carl Melis^{1,10}, G. Duchêne^{2,3}, Laura Chomiuk^{4,5}, Patrick Palmer⁶, M. D. Perrin⁷, S. T. Maddison⁸, F. Ménard³, K. Stapelfeldt⁹, C. Pinte³, G. Duvert³

cmelis@ucsd.edu

ABSTRACT

We are undertaking a multi-frequency Expanded Very Large Array (EVLA) survey of edge-on protoplanetary disks to probe the growth of solids in each disk, sedimentation of such material into the disk midplane, and the connection of these phenomena to the planet formation process. The projection of edge-on disk systems along our line of sight enables a study of the vertical stratification of large grains with fewer model dependencies than would be required for disks that are more face-on. Robust studies of the spatial distribution of grains up to ≈ 1 cm in size are possible with the wavelength range and sensitivity of the EVLA. In this contribution we describe target selection and observational strategies. First results concerning the Class 0 source IRAS 04368+2557 (L1527 IRS) are presented, including a study of this source's 8.46 GHz continuum variability over

¹Center for Astrophysics and Space Sciences, University of California, San Diego, CA 92093-0424, USA

²Astronomy Department, 601 Campbell Hall, University of California, Berkeley, CA 94720-3411, USA

³UJF-Grenoble 1/ CNRS-INSU, Institut de Planétologie et d'Astrophysique de Grenoble (IPAG) UMR 5274, BP 53, 38041 Grenoble Cedex 9, France

⁴Harvard-Smithsonian Center for Astrophysics, 60 Garden St., MS-66, Cambridge, MA 02138, USA

⁵A Jansky Fellow of the National Radio Astronomy Observatory

⁶Department of Astronomy and Astrophysics, University of Chicago, 5640 S. Ellis Ave., Chicago, IL 60637, USA

⁷Space Telescope Science Institute, 3700 San Martin Drive, Baltimore, MD 21231, USA

⁸Centre for Astrophysics & Supercomputing, Swinburne University, PO Box 218, Hawthorn, VIC 3122, Australia

⁹Jet Propulsion Laboratory, California Institute of Technology, Mail Stop 183-900, 4800 Oak Grove Drive, Pasadena, CA 91109, USA

¹⁰Joint NSF AAPF Fellow and CASS Postdoctoral Fellow

short and long time baselines and an indication that its protoplanetary disk may have a dearth of pebble-sized grains.

Subject headings: accretion, accretion disks — circumstellar matter — planets and satellites: formation — protoplanetary disks — stars: individual (IRAS 04368+2557) — stars: variables: T Tauri, Herbig Ae/Be

1. Introduction

Both major contending theories of planet formation, core accretion and gravitational instability, require collection of solid material into a dense mid-plane layer within circumstellar disks (e.g., Pollack *et al.* 1996; Boss 1997; Schr pler & Henning 2004, and references therein). To understand this first stage in the generation of planetary embryos we must determine the necessary conditions for grain sedimentation and if the relevant physical processes act uniformly with particle size. Numerical simulations incorporating gas drag and stellar gravity predict that larger grains are expected to settle into the disk mid-plane more efficiently than smaller grains (e.g., Barri re-Fouchet *et al.* 2005; Laibe *et al.* 2008). However, these simulations predict extremely short timescales for the growth and migration of dust particles that are inconsistent with observations, suggesting that some additional disk physics needs to be included (see Brauer *et al.* 2007). Observational results, and modeling thereof (e.g., Duch ne *et al.* 2003; Pinte *et al.* 2007), have begun to lay the foundation for grain sedimentation and its relation to grain growth, providing evidence in support of larger grains being more concentrated towards the disk mid-plane. Although these works hint that grain growth, radial migration, and sedimentation are intimately connected, observations that resolve the spatial distribution of large grains are necessary to complete this picture.

Study of the largest dust grains and their spatial distribution requires observations at long wavelengths (commensurate with grain size; e.g., Natta *et al.* 2004; Wilner *et al.* 2005; Rodmann *et al.* 2006; Lommen *et al.* 2009). Unambiguous grain vertical distribution information can only come from protoplanetary disks which are edge-on to our line of sight (Section 2). Edge-on protoplanetary disk systems imaged in scattered light typically subtend $\sim 0.3\text{--}3''$ in the vertical direction (see Table 1 references). To identify vertical grain stratification, thermal emission from disk atmosphere grains must be separated from that of grains settled to the disk mid-plane with high angular resolution observations. Hence, to study the vertical distribution of large grains, one must map edge-on disk systems with a long-baseline radio interferometer such as the NRAO¹ Expanded Very Large Array (EVLA;

¹The National Radio Astronomy Observatory is a facility of the National Science Foundation operated

Perley *et al.* 2011).

In this contribution we present an EVLA survey of edge-on protoplanetary disk systems. Target selection and observations are discussed, and first results on the source IRAS 04368+2557 are reported.

2. Sample Definition

Edge-on disks are selected because of their favorable geometry: each beam of an edge-on disk map samples a single disk altitude. From spectral index maps of edge-on disk systems we will measure the maximum grain size per synthesized beam and hence the vertical distribution of grains as a function of grain size. Some assumptions regarding disk axisymmetry may be necessary to delineate optical depth effects from true grain size variation, especially near the disk mid-plane (see also discussion in Section 4.3).

We arbitrarily restrict our sample to disks with inclination angle $\gtrsim 75^\circ$ (where 0° is face-on to our line of sight) to limit confusion between radial and altitude flux variations. All sources in our sample have been selected based on the existence of scattered light images that allow a determination of the disk inclination to a few degrees. Ultimately, such a sample will enable more powerful global panchromatic analyses (e.g., Pinte *et al.* 2008; Duchêne *et al.* 2010).

Disk systems observed in the first EVLA observing cycle are listed in Table 1.

3. Observational Strategy

Preliminary observations aim to identify microwave-bright disks for future mapping and to characterize the overall degree of grain growth for each disk system based on measurement of their long-wavelength opacity index β (where $\kappa_\nu \propto \nu^\beta$). The value of β provides information on the size of grains relative to the observing wavelength, where $\beta \lesssim 1$ indicates grains comparable to or larger than the observing wavelength (e.g., Beckwith *et al.* 1990; Mannings & Emerson 1994; Rodmann *et al.* 2006; Lommen *et al.* 2009; Ricci *et al.* 2010; Section 4.3 discusses how disk optical depth affects the determination of β). These goals require total power measurements (i.e., unresolved disk measurements) which are best done in compact array configurations.

Disk flux measurements are made at 7 and 13 mm. Robust measurement of the opacity index β requires removing emission from processes other than dust thermal emission. Young stellar objects are known to emit in the microwave due to free-free emission from ionized jets and disk-winds and gyrosynchrotron emission from coronal processes (see e.g., Osten & Wolk 2009, and references therein). Previous works have shown that free-free and gyrosynchrotron emission (hereafter non-disk emission) can contaminate the 7-13 mm wavelength region at a level that is anywhere from 0-100% of the detected flux (e.g., Natta *et al.* 2004; Rodmann *et al.* 2006). It is assumed that measurements longward of 20 mm are probing only non-disk emission (this is not always the case; see Wilner *et al.* 2005). We perform observations at both 35 and 60 mm so that there are two data points with which to determine the spectral slope of non-disk emission components.

Non-disk emission is known to be variable (e.g., Osten & Wolk 2009). Proper removal of this variable emission requires observations of the non-disk component that are as close in time as possible to observations of the disk component. To obtain quasi-simultaneous observations across all bands, we intertwined scans at 7, 13, 35, and 60 mm within a continuous observing block (which can span 3-5 hours; see Table 2). Although these disk and non-disk measurements are not perfectly simultaneous, the assumption is that averaging 35 and 60 mm scans taken over the entire observing block will yield an accurate measurement of the non-disk emission component during 7 and 13 mm scans. We test this strategy in Section 4.2.

4. Case Study: IRAS 04368+2557

Of the 11 sources observed in the first EVLA cycle, 9 were detected (Table 1). In this section observations of IRAS 04368+2557 (L1527 IRS) are presented as a case study of the methodologies outlined above.

IRAS 04368+2557 is an embedded class 0 object in the L1527 dark cloud in Taurus (White & Hillenbrand 2004). Although optically faint (e.g., White & Hillenbrand 2004), IRAS 04368+2557 is bright in the sub-millimeter (Chandler & Richer 2000; Andrews & Williams 2005), millimeter (Ohashi *et al.* 1997; Motte & André 2001), and microwave (Rodríguez & Reipurth 1998; Loinard *et al.* 2002). Millimeter and sub-millimeter results to date show that IRAS 04368+2557 is composed of a substantial envelope that is infalling onto the central source (Ohashi *et al.* 1997; Chandler & Richer 2000; Motte & André 2001; Andrews & Williams 2005). VLA imaging detects jet emission emanating from the central protostar (Rodríguez & Reipurth 1998; Reipurth *et al.* 2004) and provides evidence of a ~ 24 AU binary companion (Loinard *et al.* 2002). The disk surrounding the central source is probed most recently by Tobin *et al.*

(2010) who present $3.78\,\mu\text{m}$ imaging that resolves the inner envelope and disk structure of IRAS 04368+2557. The only unambiguous detection of disk thermal emission comes from Loinard *et al.* (2002) who resolve the disk at 7 mm. Our observations provide the first nearly simultaneous, multiband, compact configuration radio frequency observations of IRAS 04368+2557.

4.1. Observations

IRAS 04368+2557 was observed with all 27 EVLA antennas. Some details of the observations are given in Table 2. The WIDAR correlator was set up with two 128 MHz sub-bands centered on the frequencies listed in Table 2. Each sub-band had 4 polarization products (RR, LL, RL, LR) and sixty-four 2000 kHz channels. Observations at 7 and 13 mm were performed in “fast-switching” mode; target source scans were interleaved with frequent visits to a nearby calibration source to freeze out rapid atmospheric phase fluctuations. Cycle times of 2 and 4 minutes were used for 7 and 13 mm, respectively. The primary calibration source 3C286 was used to measure the complex bandpass and to set the absolute flux scale.

To probe the stability of the non-disk emission component over long and short time baselines we retrieved VLA archival 35 mm observations of IRAS 04368+2557 (see Table 2). To maintain homogeneity in this data set we only use observations performed with all VLA antennas. VLA observations were made in both circular polarizations with an effective bandwidth of 92 MHz centered at a frequency of 8.46 GHz. Data from AR0350 and AR0465 are presented in Rodríguez & Reipurth (1998) and Reipurth *et al.* (2004), respectively. All other data are unpublished to the best of our knowledge. While our reductions agree well with those of Rodríguez & Reipurth (1998), we find a significantly lower flux density for IRAS 04368+2557 than do Reipurth *et al.* (2004). Further investigation shows that our measurement is consistent with what is displayed in Figure 2 of Reipurth *et al.* (2004), but that this and our measurement are both inconsistent with what is listed in their Table 2.

All data are reduced using the Astronomical Image Processing Software (AIPS; Greisen 2003). VLA data are edited and calibrated following standard VLA data reduction procedures. EVLA data are edited and calibrated in a similar manner, except for the addition of first pass fringe fitting to set the interferometer delays (performed on the primary calibrator, 3C286) and bandpass calibration. Standard high-frequency reduction techniques are employed for 7 mm data. IRAS 04368+2557 is detected at all observed frequencies with $\gtrsim 10\sigma$ significance. We assume absolute flux density scale systematic uncertainties of 15% and 5% for 7 and 13 mm, respectively; these are included in the Table 2 uncertainties. Absolute flux densities for 35 and 60 mm are assumed to be limited by the rms noise level in CLEANed

maps. Figure 1 shows contour maps from the EVLA data; IRAS 04368+2557 is not resolved in any of the EVLA images.

4.2. Centimetric Variability

Figure 2 presents 35 mm measurements of IRAS 04368+2557 from each epoch listed in Table 2. Inter-epoch measurements are made by imaging all data obtained in the time interval listed for that epoch. Intra-epoch measurements are made by imaging the smallest time interval that yields an $\approx 10\sigma$ detection of IRAS 04368+2557.

Except for the 2002 data, no significant ($>3\sigma$) inter-epoch variability is detected. The 2002 observations were done with the most extended array configuration and emission structures could have been resolved out by the widely separated baselines resulting in lower than average flux densities. Intra-epoch measurements reveal two transient events. The first is a mini-flare observed near the end of the 26 minute long UT 1997 Aug 14 scan. The second is the radio jet detected by Reipurth *et al.* (2004) which appears only near the end of the UT 2002 Feb 08 data set. Out of eighteen ≈ 25 minute long 35 mm IRAS 04368+2557 sequences, one exhibits a flare event and one exhibits a jet event. The occurrence rate of such events in 25 minute windows is $\sim 6\%$ if the events are unique and $\sim 11\%$ if they are the same phenomenon.

Compared to previous studies of young stellar object centimetric variability (e.g., Forbrich *et al.* 2006, 2007; Choi *et al.* 2008; Osten & Wolk 2009), the results presented herein appear to agree best with the Osten & Wolk (2009) study of short and long term variability in six young stellar objects. At a wavelength of 60 mm they find that 4 out of 6 young stellar objects show short term variability and that 3 out of 6 objects show long term variability (the positive variability detections are not necessarily from the same objects in each group). Hence, their results suggest that young stellar objects appear to be just as likely to have short term variability as they are to exhibit long term variability. Such conclusions seem to contradict the results of Forbrich *et al.* (2006, 2007) and Choi *et al.* (2008), where it is found that there are generally lower levels of variability on shorter timescales. However, of the above mentioned studies, only Osten & Wolk (2009) analyze variability on intra-epoch (less than day) timescales. It could be the case that even seemingly stable sources have sporadic variability that can only be probed on the shortest timescales. If the event occurrence rate derived above for IRAS 04368+2557 is representative of stars in the same class, then such sources might exhibit short-duration flares in as many as one out of ten 25 minute observing windows. However, since less than ten sources have been probed on intra-epoch timescales, it is likely premature to extend their results to other sources. Monitoring similar

to that presented here and in Osten & Wolk (2009) of new and previously studied young stellar objects can further address variability timescales and strength in a more statistical sense.

For weak flare events like those detected here, averaging over the duration of an observing block sufficiently suppresses the flare effect. Stronger flares can likely be identified by analyzing all data in a time-series fashion. No strong flares are present in the EVLA data.

4.3. Disk Emission Spectral Index

Figure 3 shows the EVLA flux measurements of IRAS 04368+2557 with literature measurements at millimeter and sub-millimeter wavelengths. The 450 and 850 μm measurements (Andrews & Williams 2005) were made with beam sizes of 9 and 15", respectively, while the 1.3 mm measurement (Motte & André 2001) was made with a beam size of 11". The 2.7 mm measurement (Ohashi *et al.* 1997) was made with a synthesized beam size of 6" \times 4.9" (PA +163°).

The non-disk emission component is fit with $\alpha_{35-60\text{mm}}=0.33\pm0.17$ (where α is the spectral index $F_\nu \propto \nu^\alpha$), consistent with non-disk indices assumed by Rodmann *et al.* (2006). An extrapolation of the non-disk emission fit is subtracted from 7 and 13 mm measurements; uncertainties of each flux measurement and the spectral index are propagated into the corrected flux uncertainties. We calculate for IRAS 04368+2557 $\alpha_{0.45-1\text{mm}}=1.93\pm0.25$ and $\alpha_{1-7\text{mm}}=2.87\pm0.17$ using the corrected 7 mm flux density. We use different spectral indices for wavelengths $\lesssim 1\text{ mm}$ and $\gtrsim 1\text{ mm}$ since single power-law fits to all sub-millimeter and millimeter data points are discrepant with the 450 μm flux measurement at the $\approx 5\sigma$ level. The spectral index from 450 μm to 1.3 mm is consistent with Rayleigh-Jeans emission suggesting that the disk is opaque at these wavelengths. In the case of the 450 μm to 2.7 mm measurements, there is likely contamination from extended envelope structure detected around IRAS 04368+2557 (see below and Ohashi *et al.* 1997; Chandler & Richer 2000; Motte & André 2001; Andrews & Williams 2005). If these measurements are contaminated by envelope emission, then the disk-only $\alpha_{1-7\text{mm}}$ is smaller (flatter) than the value quoted above. It is noted that the EVLA 7 mm flux measurement is roughly consistent with the total flux density estimated for the resolved structures detected by Loinard *et al.* (2002). This suggests that the disk structure is fairly compact (relative to the envelope structure), in agreement with scattered light images presented by Tobin *et al.* (2010). IRAS 04368+2557 is resolved at wavelengths shorter than 7 mm with beam sizes larger than the EVLA 7 mm synthesized beam implying that those flux measurements include envelope emission. Synthesis of the above suggests that accurate measurement of grain growth from spectral indices

requires data sets having beam sizes comparable to the disk angular size when contaminating sources are present.

Extracting an opacity index β from the above measured $\alpha_{1-7\text{mm}}$ is complicated not only by envelope contamination but also by edge-on disk geometry. When calculating β one must account for optically thick inner disk emission sampled by the flux measurements. Should no optically thick emission be present, then β is simply $\alpha_{1-7\text{mm}} - 2$. In the case that optically thick emission is present in the measurements, β takes the form of $(1 + \Delta)(\alpha_{1-7\text{mm}} - 2)$ where Δ is the ratio of optically thick to optically thin emission (Beckwith *et al.* 1990). As discussed above, the disk orbiting IRAS 04368+2557 appears to be completely opaque out to wavelengths as long as ~ 1 mm. Thus, significant optically thick emission may be present even at wavelengths near 10 mm. Estimates of Δ are typically made assuming some disk mass density profile and by measuring the temperature profile from spectral indices and disk flux levels in the optically thick wavelength regime (Beckwith *et al.* 1990; Rodmann *et al.* 2006). However, Equation 10 of Beckwith *et al.* (1990) shows that mapping spectral indices and disk flux levels into temperature profiles is confounded when disks are nearly edge-on. Modeling of edge-on disk spectral energy distributions and resolved images can recover their true disk temperature profiles. Due to this additional modeling and envelope contamination uncertainties, we leave derivation of the opacity index for the IRAS 04368+2557 disk to future works.

The 13 mm measurement appears to fall short of the $\nu^{2.87}$ fit after being corrected for non-disk emission. This flux deficit suggests a break in the disk emission spectral index from 7 to 13 mm, but is marginally significant. If envelope contamination is present as discussed above, then its removal would increase the significance of the deficient corrected 13 mm measurement. Comparison to other protoplanetary disk systems shows that such a break would be unusual (e.g., Wilner *et al.* 2005; Rodmann *et al.* 2006; Lommen *et al.* 2009) and suggestive of a cut-off near pebble-sizes in the disk grain size distribution. If these characteristics of IRAS 04368+2557 are confirmed, then there may be a connection between its potential ~ 24 AU binary companion (Loinard *et al.* 2002), its apparent 7 mm outer disk truncation (Loinard *et al.* 2002), and its possible lack of large disk grains.

5. Conclusions

We are carrying out an Expanded Very Large Array program to map the vertical distribution of large grains in edge-on protoplanetary disks. The ultimate goal of this survey is to study grain growth and sedimentation as the first stages of planet formation. Our compact array observational strategy aims to provide accurate disk thermal emission measurements

in the microwave by sampling non-disk emission in concert with disk measurements. First EVLA results for IRAS 04368+2557 show that the protoplanetary disk around this source is likely optically thick out to millimeter wavelengths and that it may have a dearth of “pebble-sized” grains.

We thank the anonymous referee for comments that helped improve this work. C.M. acknowledges support from the National Science Foundation under award No. AST-1003318. M.D.P. was supported by NSF Postdoctoral Fellowship No. AST-0702933. F.M., C.P., and G.D. acknowledge PNPS of CNRS/INSU, and ANR (contract ANR-07-BLAN-0221) of France for financial support. C.P. acknowledges funding from the European Commission’s 7th Framework Program (contract PIEF-GA-2008-220891) and from ANR under contract ANR-2010-JCJC-0504-01.

Facilities: EVLA (), VLA ()

REFERENCES

- Andrews, S. M. & Williams, J. P. 2005, *ApJ*, **631**, 1134
- Appenzeller, I., Bertout, C., & Stahl, O. 2005, *A&A*, **434**, 1005
- Bally, J., Devine, D., Fesen, R. A., & Lane, A. P. 1995, *ApJ*, **454**, 345
- Barrière-Fouchet, L., Gonzalez, J., Murray, J. R., Humble, R. J., & Maddison, S. T. 2005, *A&A*, **443**, 185
- Beckwith, S. V. W., Sargent, A. I., Chini, R. S., & Guesten, R. 1990, *AJ*, **99**, 924
- Bontemps, S., *et al.* 2001, *A&A*, **372**, 173
- Boss, A. P. 1997, *Science*, **276**, 1836
- Brandner, W., *et al.* 2000, *A&A*, **364**, L13
- Brauer, F., Dullemond, C. P., Johansen, A., Henning, T., Klahr, H., & Natta, A. 2007, *A&A*, **469**, 1169
- Bujarrabal, V., Young, K., & Castro-Carrizo, A. 2009, *A&A*, **500**, 1077
- Bujarrabal, V., Young, K., & Fong, D. 2008, *A&A*, **483**, 839
- Chandler, C. J. & Richer, J. S. 2000, *ApJ*, **530**, 851

- Choi, M., Hamaguchi, K., Lee, J., & Tatematsu, K. 2008, *ApJ*, **687**, 406
- Devine, D., Bally, J., Chiriboga, D., & Smart, K. 2009, *AJ*, **137**, 3993
- Duchêne, G., Bontemps, S., Bouvier, J., André, P., Djupvik, A. A., & Ghez, A. M. 2007, *A&A*, **476**, 229
- Duchêne, G., Ménard, F., Stapelfeldt, K., & Duvert, G. 2003, *A&A*, **400**, 559
- Duchêne, G., *et al.* 2010, *ApJ*, **712**, 112
- Forbrich, J., Preibisch, T., & Menten, K. M. 2006, *A&A*, **446**, 155
- Forbrich, J., *et al.* 2007, *A&A*, **464**, 1003
- Greisen, E. W. 2003, *Information Handling in Astronomy - Historical Vistas*, **285**, 109
- Grosso, N., Alves, J., Wood, K., Neuhäuser, R., Montmerle, T., & Bjorkman, J. E. 2003, *ApJ*, **586**, 296
- Krist, J. E., *et al.* 1998, *ApJ*, **501**, 841
- Laibe, G., Gonzalez, J., Fouchet, L., & Maddison, S. T. 2008, *A&A*, **487**, 265
- Loinard, L., Rodríguez, L. F., D'Alessio, P., Wilner, D. J., & Ho, P. T. P. 2002, *ApJ*, **581**, L109
- Lommen, D., Maddison, S. T., Wright, C. M., van Dishoeck, E. F., Wilner, D. J., & Bourke, T. L. 2009, *A&A*, **495**, 869
- Mannings, V. & Emerson, J. P. 1994, *MNRAS*, **267**, 361
- Motte, F. & André, P. 2001, *A&A*, **365**, 440
- Natta, A., Testi, L., Muzerolle, J., Randich, S., Comerón, F., & Persi, P. 2004, *A&A*, **424**, 603
- Ohashi, N., Hayashi, M., Ho, P. T. P., & Momose, M. 1997, *ApJ*, **475**, 211
- Osten, R. A. & Wolk, S. J. 2009, *ApJ*, **691**, 1128
- Perley, R. A., Chandler, C. J., Butler, B. J., & Wrobel, J. M. 2011, *ApJ*, in press
- Perrin, M. D., Duchêne, G., Kalas, P., & Graham, J. R. 2006, *ApJ*, **645**, 1272
- Pinte, C., Fouchet, L., Ménard, F., Gonzalez, J., & Duchêne, G. 2007, *A&A*, **469**, 963

- Pinte, C., *et al.* 2008, *A&A*, **489**, 633
- Pollack, J. B., Hubickyj, O., Bodenheimer, P., Lissauer, J. J., Podolak, M., & Greenzweig, Y. 1996, *Icarus*, **124**, 62
- Reipurth, B., Rodríguez, L. F., Anglada, G., & Bally, J. 2004, *AJ*, **127**, 1736
- Ricci, L., Testi, L., Natta, A., Neri, R., Cabrit, S., & Herczeg, G. J. 2010, *A&A*, **512**, A15+
- Rodmann, J., Henning, T., Chandler, C. J., Mundy, L. G., & Wilner, D. J. 2006, *A&A*, **446**, 211
- Rodríguez, L. F. & Reipurth, B. 1998, *Rev. Mexicana Astron. Astrofis.*, **34**, 13
- Ruiz, M. T., *et al.* 1987, *ApJ*, **316**, L21
- Sauter, J., *et al.* 2009, *A&A*, **505**, 1167
- Schräpler, R. & Henning, T. 2004, *ApJ*, **614**, 960
- Stapelfeldt, K. R., Ménard, F., Watson, A. M., Krist, J. E., Dougados, C., Padgett, D. L., & Brandner, W. 2003, *ApJ*, **589**, 410
- Stark, D. P., Whitney, B. A., Stassun, K., & Wood, K. 2006, *ApJ*, **649**, 900
- Tobin, J. J., Hartmann, L., & Loinard, L. 2010, *ApJ*, **722**, L12
- van Kempen, T. A., van Dishoeck, E. F., Salter, D. M., Hogerheijde, M. R., Jørgensen, J. K., & Boogert, A. C. A. 2009, *A&A*, **498**, 167
- Vieira, S. L. A., *et al.* 2003, *AJ*, **126**, 2971
- White, R. J. & Hillenbrand, L. A. 2004, *ApJ*, **616**, 998
- Wilner, D. J., D’Alessio, P., Calvet, N., Claussen, M. J., & Hartmann, L. 2005, *ApJ*, **626**, L109
- Wolf, S., Padgett, D. L., & Stapelfeldt, K. R. 2003, *ApJ*, **588**, 373

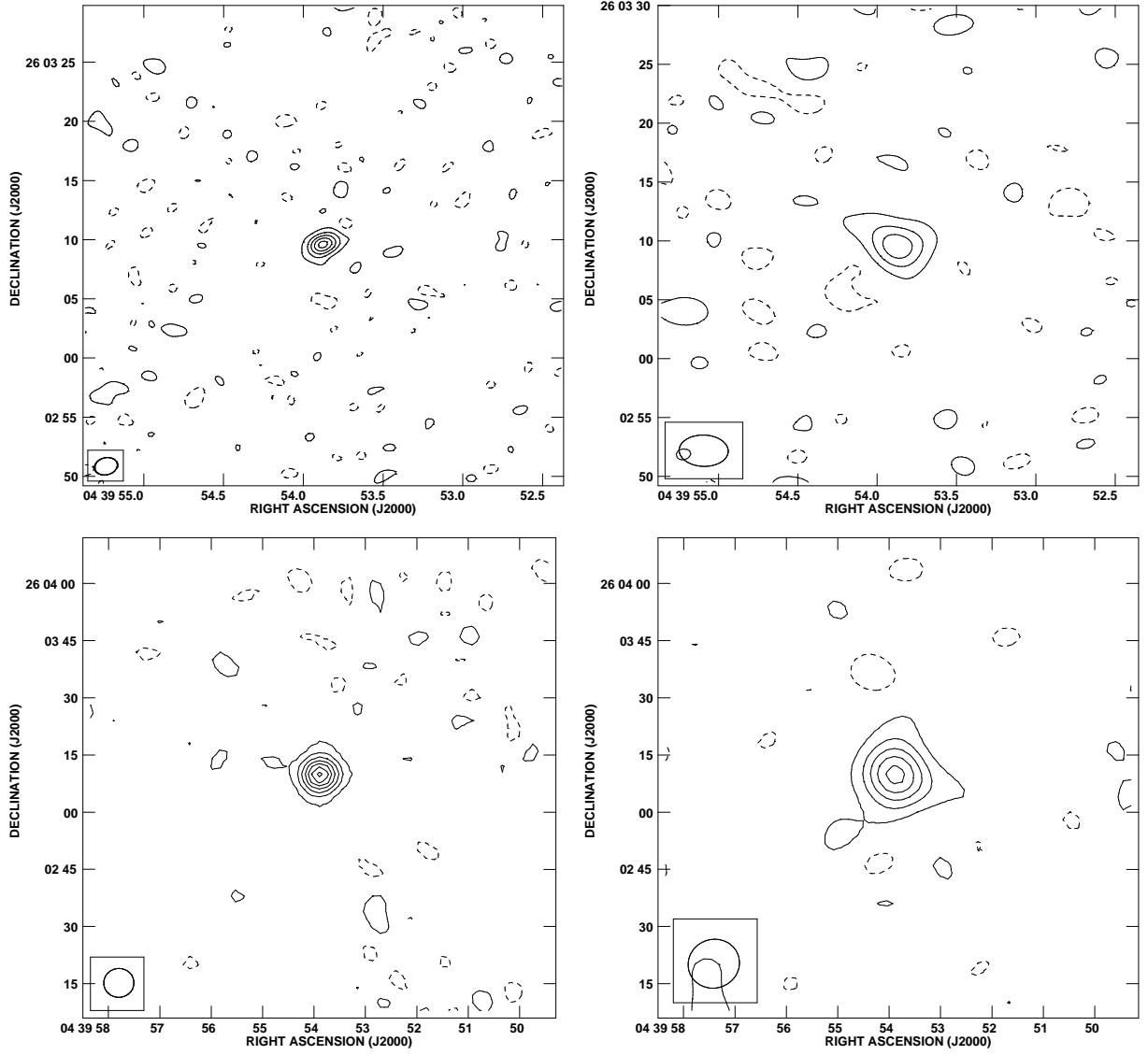


Fig. 1.— EVLA images of IRAS 04368+2557. The top row shows 7 mm (left) and 13 mm (right) maps while the bottom row shows 35 mm (left) and 60 mm (right) maps. Half-power contours of the beam are shown in the bottom left of each plot, beam sizes can be found in Table 2. Contour levels start at -2 times the map rms noise level (dashed contours) and increment by 4 times the map rms noise level (0.2 mJy, 0.1 mJy, 30 μ Jy, and 33 μ Jy for 7, 13, 35, and 60 mm respectively).

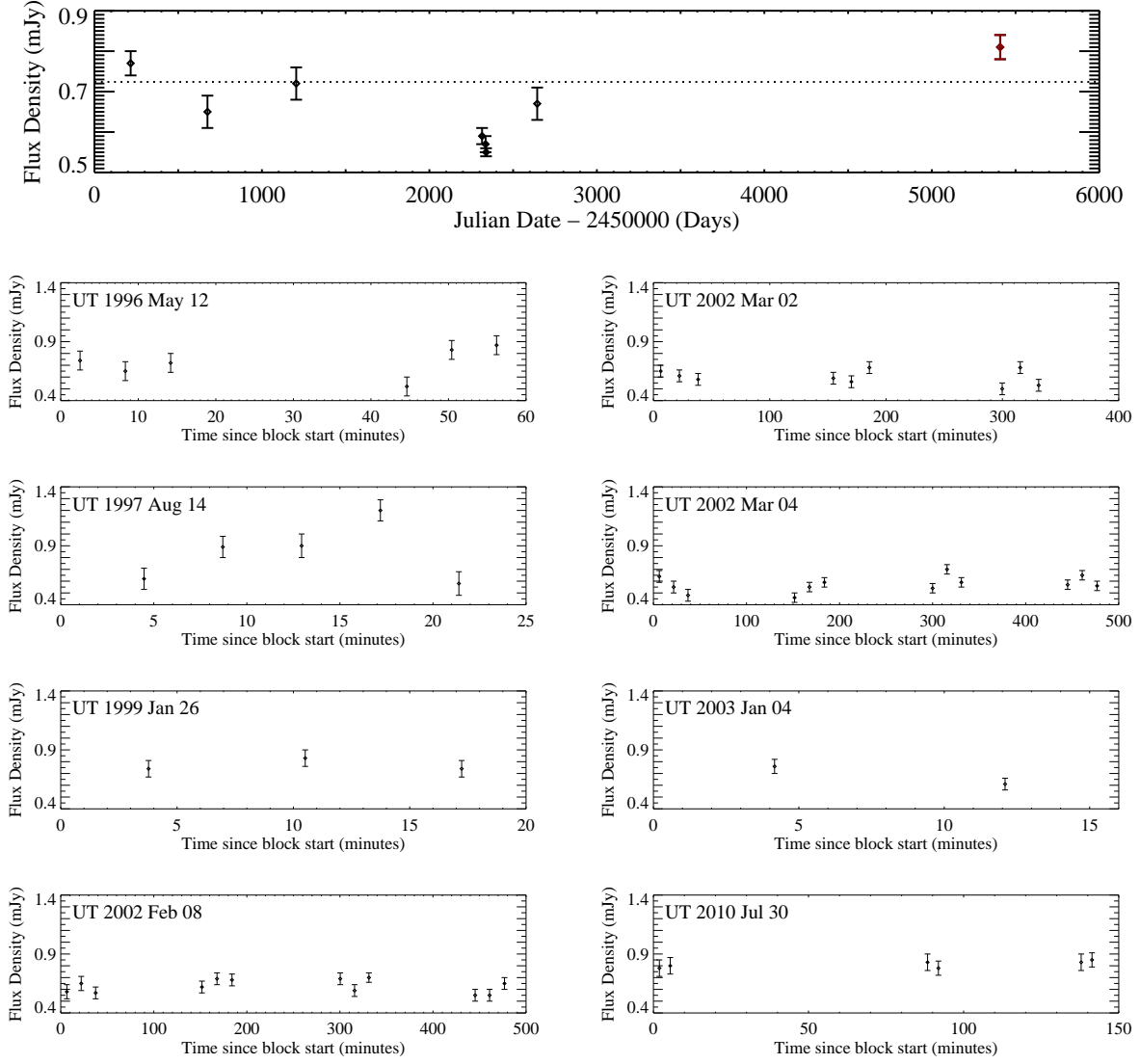


Fig. 2.— X-band (8.46 GHz; 35 mm) measurements of IRAS 04368+2557. The top panel presents inter-epoch measurements (one measurement for each date listed in Table 2; EVLA data are in red). The dotted line is the mean flux level of all compact array measurements. The lower panels show intra-epoch measurements for the date listed in each plot. The abscissa shows time since the Table 2 UT start time of each epoch. Note the mini-flare detected on UT 1997 Aug 14.

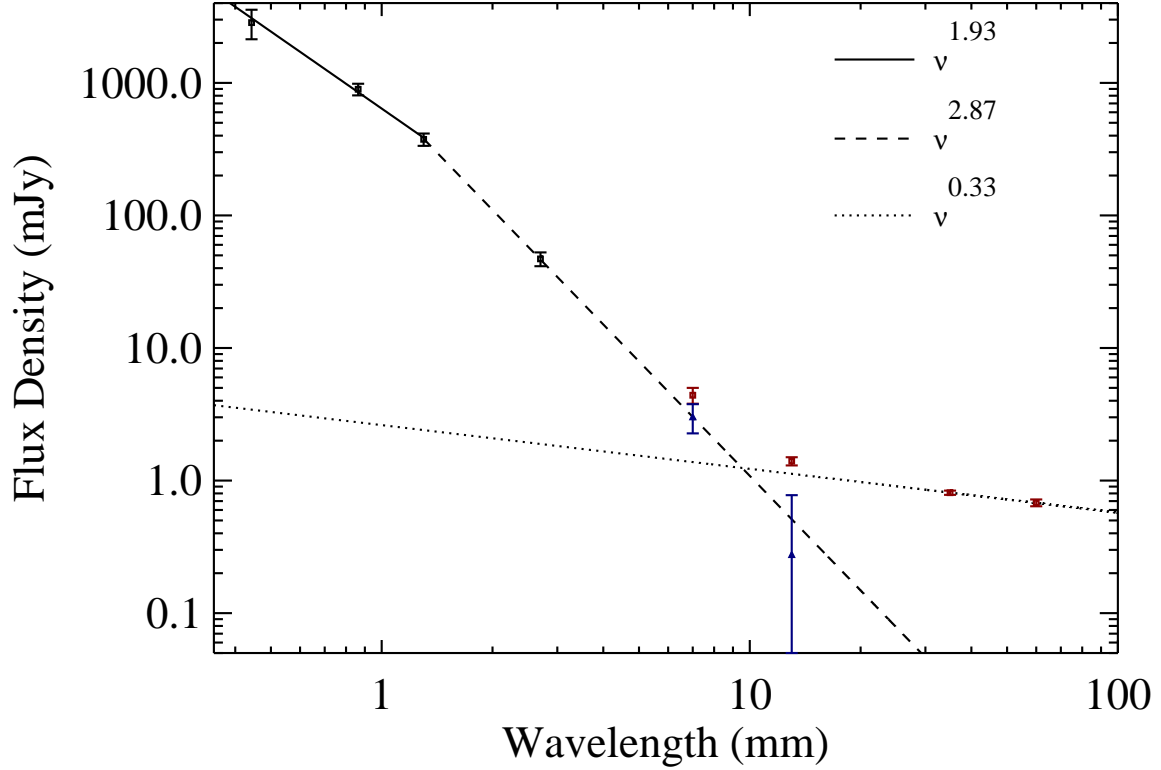


Fig. 3.— IRAS 04368+2557 long-wavelength spectral energy distribution. Uncertainties are 1σ . Red data points longward of 3 mm are EVLA data. See Section 4.3 and Table 2 for measurement beam sizes. The $450\ \mu\text{m}$ to 2.7 mm measurement errors include 10-25% absolute flux scale systematic uncertainties. The dotted line fits the 35 and 60 mm measurements which are assumed to be entirely due to non-disk emission (this fit does not include the 13 mm data point). Lower, blue triangle data points are corrected measurements (Section 4.3); the 13 mm uncertainty extends to 0. The $\nu^{2.87}$ fit does not include the corrected 13 mm measurement. See Section 4.3 for a discussion of the two disk emission spectral indices used.

Table 1. EVLA D-array Observed Targets

Name	RA (J2000 Phase Center)	DEC	Spectral Type	Disk Class	Inclination (°)	Disk Size ^a (″)	Ref	Detected? ^b
Haro 6–5B	04 22 01.0	+26 57 35	K5	II	75	4	1,2,3	Y
IRAS 04302+2247	04 33 16.5	+22 53 20	—	I	87	2	1,3,4	Y
HV Tau C	04 38 35.5	+26 10 41	M0	II	84	0.7	5,6,7	Y
IRAS 04368+2557	04 39 53.6	+26 03 06	—	0	85	1	1,8	Y
CB 26	04 59 50.7	+52 04 44	—	I-II	85	2.8	9	Y
PDS 144 N ^c	15 49 15.4	−26 00 52	A2	II	83	0.8	10,11	Y
LFAM1 ^d	16 26 21.8	−24 22 51	—	I	85	1	12,13,14	Y
Oph E MM3	16 27 05.9	−24 37 08	—	II	87	1	12,15	Y
Flying Saucer	16 28 13.2	−24 31 39	—	II	86	4.3	12,16	N
Gomez’s Hamburger	18 09 13.4	−32 10 50	A0	II	84	12	17,18,19	Y
HH 200	20 57 06.6	+77 36 56	—	II	87	1.5	20,21	N

References. — (1) White & Hillenbrand (2004), (2) Krist *et al.* (1998), (3) Stark *et al.* (2006), (4) Wolf *et al.* (2003), (5) Appenzeller *et al.* (2005), (6) Stapelfeldt *et al.* (2003), (7) Duchêne *et al.* (2010), (8) Tobin *et al.* (2010), (9) Sauter *et al.* (2009), (10) Vieira *et al.* (2003), (11) Perrin *et al.* (2006), (12) van Kempen *et al.* (2009), (13) Bontemps *et al.* (2001), (14) Duchêne *et al.* (2007), (15) Brandner *et al.* (2000), (16) Grosso *et al.* (2003), (17) Ruiz *et al.* (1987), (18) Bujarrabal *et al.* (2008), (19) Bujarrabal *et al.* (2009), (20) Bally *et al.* (1995), (21) Devine *et al.* (2009).

^aDisk angular diameter from optical scattered light or millimeter imaging. In its most extended array configu-

ration the EVLA has synthesized beam sizes at 7 and 13 mm of $\approx 0.043''$ and $0.089''$, respectively.

^bIf source was detected in 7 and 13 mm observations.

^c7 mm observations with the VLA in the CnB array configuration; no 13 mm observations were done.

^dArchival 7 mm observations with the VLA, program AR0698; no 13 or 60 mm observations were done.

Table 2. IRAS 04368+2557 Observations

Project	Date (UT start)	ν (GHz)	λ (mm)	Flux Density (mJy)	Beam Size ($''$)	Observation Interval (UT time)	TOS ^a (minutes)	Calibrator
EVLA Observations								
AM1017	30 Jul 2010	43.3	7	4.4 \pm 0.6	1.96 \times 1.44 (PA -76.1°)	11:56–13:32	22	J0438+300
AM1017	30 Jul 2010	22.5	13	1.4 \pm 0.1	4.16 \times 2.66 (PA $+88.3^\circ$)	11:41–13:16	26	J0431+206
AM1017	30 Jul 2010	8.5	35	0.81 \pm 0.03	7.90 \times 7.56 (PA -85.4°)	11:19–13:42	21	J0431+206
AM1017	30 Jul 2010	5.0	60	0.68 \pm 0.04	13.54 \times 12.74 (PA -70.4°)	11:29–13:52	21	J0431+206
VLA Observations								
AS0711	04 Jan 2003	8.5	35	0.67 \pm 0.04	2.45 \times 2.18 (PA -51.3°)	06:48–07:04	16.17	J0431+206
AR0465	04 Mar 2002	8.5	35	0.55 \pm 0.01	0.23 \times 0.22 (PA $+89.8^\circ$) ^b	20:59–05:02	159.5	J0403+260
AR0465	02 Mar 2002	8.5	35	0.57 \pm 0.02	—	00:06–05:44	116.83	J0403+260
AR0465	08 Feb 2002	8.5	35	0.59 \pm 0.02	—	23:03–07:06	156.5	J0403+260
AS0653	26 Jan 1999	8.5	35	0.72 \pm 0.04	2.72 \times 2.44 (PA $+70.7^\circ$)	06:29–06:50	20.5	J0431+206
AE0112	14 Aug 1997	8.5	35	0.65 \pm 0.04	2.28 \times 2.20 (PA $+39.0^\circ$)	12:43–13:09	25.67	J0431+206
AR0350	12 May 1996	8.5	35	0.77 \pm 0.03	7.79 \times 2.64 (PA -86.5°)	18:52–19:51	35.5	J0403+260

^aTime on source; aggregate of scan lengths only, does not account for slewing/settling of telescopes.

^bSynthesized beam size for all AR0465 data.